Journal of The Electrochemical Society, **156** (11) A949-A957 (2009)
0013-4651/2009/156(11)/A949/9/$25.00 © The Electrochemical Society

The Role of Coherency Strains on Phase Stability in Li_xFePO_4: Needle Crystallites Minimize Coherency Strain and Overpotential

A. Van der Ven,[a,z] K. Garikipati,[b] S. Kim,[b] and M. Wagemaker[c]

[a]*Department of Materials Science and Engineering and* [b]*Department of Mechanical Engineering, The University of Michigan, Ann Arbor, Michigan 48109, USA*
[c]*Department of Radiation, Radionuclides and Reactors, Faculty of Applied Sciences, Delft University of Technology, 2629JB Delft, The Netherlands*

We investigate the role of coherency strains on the thermodynamics of two-phase coexistence during Li (de)intercalation of Li_xFePO_4. We explicitly account for the anisotropy of the elastic moduli and analytically derive coupled chemical and mechanical equilibrium criteria for two-phase morphologies observed experimentally. Coherent two-phase equilibrium leads to a variable voltage profile of individual crystallites within the two-phase region as the dimensions of the crystallite parallel to the interface depend on the phase fractions of the coexisting phases. With a model free energy for Li_xFePO_4, we illustrate the effect of coherency strains on the compositions of the coexisting phases and on the voltage profile. We also show how coherency strains can stabilize intermediate solid solutions at low temperatures if phase separation is restricted to Li diffusion along the *b*-axis of olivine Li_xFePO_4. A finite element analysis shows that long needlelike crystallites with the long axis parallel to the *a* lattice vector of Li_xFePO_4 minimize coherency strain energy. Hence, needlelike crystallites of $LiFePO_4$ reduce the overpotential needed for Li insertion and removal and minimize mechanical damage, such as dislocation nucleation and crack formation, resulting from large coherency strain energies.
 [DOI: 10.1149/1.3222746]

Manuscript submitted April 21, 2009; revised manuscript received June 25, 2009. Published October 1, 2009.

The kinetics of intercalation processes in the electrode materials of primary and secondary batteries involves both diffusion and phase transformations.[1-6] The first-order phase transformations that occur during the insertion or removal of Li usually result in only slight structural modifications of the host.[7-12] As a result, the transformations proceed by the passage of coherent or semicoherent interfaces that separate the new stable phases from the metastable phase. Any difference in lattice parameters between the two phases participating in the phase transformation, however, introduces coherency strains, which affect thermodynamic potentials such as the Li chemical potential and the overall free energy. This, in turn, can modify the composition bounds of any two-phase coexistence regions as well as the voltage profile for cathode compositions where two-phase coexistence occurs and may even alter phase stability qualitatively.

Coherency strains are especially important in determining the two-phase equilibrium in the Li_xFePO_4 system, as was made evident by the discovery of Chen et al.[13] of a peculiar two-phase morphology within large, chemically delithiated crystallites of Li_xFePO_4. Li diffusion in Li_xFePO_4 is restricted to one-dimensional channels parallel to the *b*-direction of the orthorhombic (*Pnma*, space group 62) Li_xFePO_4 crystal structure.[14] An elementary analysis of phase separation would therefore suggest that the interface separating Li-poor $Li_\varepsilon FePO_4$ from Li-rich $Li_{1-\delta}FePO_4$, where ε and δ are both small, should be perpendicular to the *b*-direction (i.e., parallel to the *ac* plane), as this would allow a uniform extraction (insertion) of Li ions from (in) the surfaces perpendicular to the diffusion direction. Transmission electron microscopy (TEM) observations of chemically oxidized large platelike crystallites, however, have shown that the interfaces separating the $Li_\varepsilon FePO_4$ and $Li_{1-\delta}FePO_4$ phases within the crystallites of Li_xFePO_4 are perpendicular to the *a*-direction (parallel to the *bc* plane).[13] Chen et al. argued that this morphology should minimize the elastic strain energy, allowing the crystal to relax along the *a*-direction of the orthorhombic cell, which varies by almost 5% between Li-poor $Li_\varepsilon FePO_4$ and Li-rich $Li_{1-\delta}FePO_4$.[13]

Meethong et al.[15,16] recently highlighted the importance of coherency strains on the rate capabilities of $LiFePO_4$ crystallites with differing two-phase solubility limits, showing that the nucleation and growth kinetics depend strongly on the misfit strains of the first-order phase transformation in Li_xFePO_4. The observed decrease in the miscibility gap was argued to be due to strain and surface energy and stress. They also compared the elastic strain energy of the core/shell and spherical cap two-phase morphologies within spherical crystallites, finding that the strain energy incurred by the core/shell morphology is significantly more costly than the spherical cap morphology. This work clearly demonstrated the importance of strain energy in selecting the phase transformation morphology during the intercalation processes.

Many morphologies of two-phase coexistence are geometrically possible at intermediate Li concentration in Li_xFePO_4. Several simple ones are illustrated in Fig. 1 for a crystallite having a rectangular prism shape. While a homogeneous distribution of Li throughout the crystallite is only stable for dilute or very high Li concentrations at room temperature, a complete solid solution for all *x* between 0 and 1 in Li_xFePO_4 is stable above 520 K.[17,18] Two-phase coexistence can be derived from a homogeneous crystallite either through the electrochemical removal or insertion of Li ions, or through the cooling of a high temperature solid solution with intermediate Li composition. For the Li_xFePO_4 system, we denote Li-poor $Li_\varepsilon FePO_4$ as the α-phase and Li-rich $Li_{1-\delta}FePO_4$ as the β-phase. If many crystallites are present, which can exchange Li ions among each other, two-phase coexistence can be realized by having a subset of crystallites exist as α while the others exist as β.[19] We refer to this state as an incoherent two-phase mixture, and its free energy is simply the weighted average of the free energies of each individual phase α and β. If two-phase coexistence occurs within the same crystallite, coherency strain energy becomes important. Figure 1 illustrates two important coherent two-phase morphologies for Li_xFePO_4. Morphology I is similar to that observed by Chen et al.[13] in chemically delithiated Li_xFePO_4 crystallites and has the interface separating α and β parallel to the *bc* plane (perpendicular to the *a*-axis). Morphology II has the interface between α and β parallel to the *ac* plane (perpendicular to the *b*-axis) and would emerge if phase separation occurred in the crystallographic direction of Li diffusion (*b* lattice vector).

While generally recognized as important, the effect of coherency strains on two-phase equilibrium is rarely taken into explicit consideration. Cahn, early on, explored the role of coherency strains on two-phase equilibrium, initially in the context of spinodal decomposition close to the critical point of a miscibility gap.[20] Williams[21,22]

[z] E-mail: avdv@umich.edu

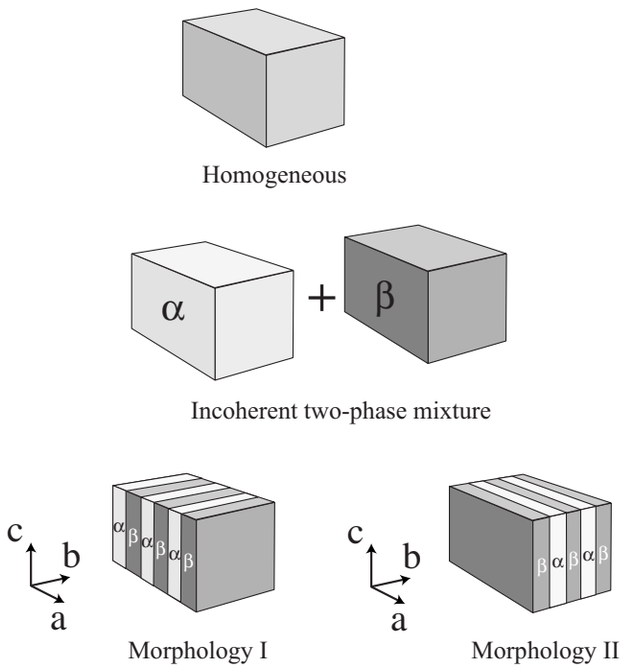

Figure 1. Various morphologies within a cathode crystallite are possible. Insertion of Li into a host such as $FePO_4$ can lead to a homogeneous distribution of Li ions within the crystallite, as observed at high temperatures in Li_xFePO_4. At low temperatures, two-phase coexistence between a Li-poor α-$Li_\varepsilon FePO_4$ phase and a Li-rich β-$Li_{1-\delta}FePO_4$ phase is thermodynamically stable. Two-phase coexistence can occur incoherently whereby a subset of electrode crystallites is in the α-phase and the remainder is in the β-phase. Two-phase coexistence can also occur within the same crystallite, as illustrated by morphologies I and II.

subsequently pointed out differences in thermodynamic equilibrium criteria between coherent two-phase coexistence and incoherent/fluid two-phase coexistence for substitutional solids, while Larche and Cahn[23-26] developed a systematic thermodynamic formalism that incorporates coherency strains in analyses of chemical equilibrium in substitutional and interstitial solids. Johnson and co-workers[27-30] expanded on this work, recently publishing an excellent and comprehensive review paper on the topic.[30]

Much of the past work on coherent equilibrium has focused on substitutional solids, while intercalation compounds should be viewed as interstitial solids in which guest ions, such as Li, occupy the interstitial sites of a relatively open host structure. Recently, the effect of coherency strains in interstitial solids has been investigated in the context of hydrogen sorption in metal hydrides, assuming isotropic elasticity.[31,32] Here, we derive general equilibrium criteria for coherent two-phase coexistence in interstitial Li-intercalation compounds using the Li_xFePO_4 system as a specific example. We derived equilibrium criteria that explicitly account for the two-phase morphology recently observed by Chen et al.[13] The general equilibrium equations incorporate the anisotropy of the elastic constants arising from the orthorhombic symmetry of the Li_xFePO_4 crystal structure.[33]

We show how coherency strain can modify solubility limits of two-phase coexistence and introduce hysteresis in the voltage curve. Within the two-phase coexistence region, the presence of coherency strains results in an equilibrium voltage curve for individual crystallites that depends on the phase fraction, as the dimensions of the crystallite and hence the thermodynamic boundary conditions of the system depend on the relative amounts of the coexisting phase in coherent equilibrium. We also show that in the presence of coherency strains, the free energy of a two-phase mixture in the Li_xFePO_4 system is minimized by a morphology in which the interface is perpendicular to the *a* lattice parameter, as opposed to the kinetically more facile morphology having an interface perpendicular to the *b*-direction corresponding to the direction of Li diffusion.

The thermodynamic effects of coherency strains also allow us to rationalize the more recent observations of Chen et al.[34] on large quenched crystallites in which a high temperature solid solution is stabilized indefinitely at room temperature. Li_xFePO_4 has a complex electronic structure, involving localized electronic states that couple to Li-vacancy disorder,[35,36] and is responsible for unique finite temperature thermodynamic properties.[37] Phase diagram measurements by Delacourt et al.[17] and Dodd et al.,[18] as well as a first-principles study by Zhou et al.,[37] show that while Li_xFePO_4 forms a solid solution at high temperature, it decomposes to a two-phase mixture of Li-poor $Li_\varepsilon FePO_4$ and Li-rich $Li_{1-\delta}FePO_4$ upon cooling, not through a miscibility gap but rather through a eutectoid reaction at approximately 200°C with a eutectoid composition $x = 0.6$.[18] The recent studies of Chen et al.[34] on large quenched particles suggest that phases having the eutectoid composition can be quenched to room temperature and do not decompose over time to form a two-phase mixture of Li-poor $Li_\varepsilon FePO_4$ and Li-rich $Li_{1-\delta}FePO_4$. Here, we show how coherency strains could be responsible for stabilizing Li_xFePO_4 at intermediate Li concentrations.

As a final result, we show that crystallites having a needle shape with the longest length parallel to the *a* lattice vector of the orthorhombic cell minimize the strain energy incurred during the two-phase coexistence, thereby reducing the required overpotential for the α to β transformation as well as the mechanical damage[38] during cycling.

Free Energy of Coherent Two-Phase Coexistence within an Orthorhombic Crystallite

We considered a crystallite having a rectangular prism shape and a simple two-phase morphology with phase fractions ϕ^α and ϕ^β for the α- and β-phases, as illustrated in Fig. 1. The total number of interstitial Li sites within the crystallite is denoted by M such that $M\phi^\alpha$ is the number of interstitial sites within the α-phase and $M\phi^\beta$ is the number of interstitial sites in the β-phase. If the total number of Li ions within the crystallite is N, a fraction N^α is distributed within the α-phase and the remaining $N^\beta = N - N^\alpha$ resides in the β-phase. In terms of these variables, the Li concentration within the α (β)-phase can then be written as $x^\alpha = N^\alpha/M\phi^\alpha$ ($x^\beta = N^\beta/M\phi^\beta$), while the overall Li concentration of the crystallite $x = N/M$ is related to the phase fractions and concentrations within the α- and β-phases according to

$$x = \phi^\alpha x^\alpha + \phi^\beta x^\beta \qquad [1]$$

The dimensions of the crystallite depend on the Li concentrations and phase fractions of the α- and β-phases. To describe the changes in the dimensions with Li concentration and phase fraction, we work within a Lagrangian description[30] and express strains relative to the equilibrium volume of a single phase crystallite having a concentration $x = 0$. The strain of the crystal along a particular direction (taking out rigid rotation and in the absence of shear) then becomes

$$\tilde{\varepsilon}_i = \frac{L_i - L_i^0}{L_i^0} \qquad [2]$$

where L_i is the length of the deformed crystalline along direction i, while L_i^0 is the length of the undeformed crystallite along i when $x = 0$. We label the six independent strains in terms of one index according to the following convention of Nye:[39] $\tilde{\varepsilon}_1 = \tilde{\varepsilon}_{11}$, $\tilde{\varepsilon}_2 = \tilde{\varepsilon}_{22}$, $\tilde{\varepsilon}_3 = \tilde{\varepsilon}_{33}$, $\tilde{\varepsilon}_4 = 2\tilde{\varepsilon}_{23} = 2\tilde{\varepsilon}_{32}$, $\tilde{\varepsilon}_5 = 2\tilde{\varepsilon}_{13} = 2\tilde{\varepsilon}_{31}$, and $\tilde{\varepsilon}_6 = 2\tilde{\varepsilon}_{12} = 2\tilde{\varepsilon}_{21}$.

The strain $\tilde{\varepsilon}_i$, relative to the reference volume at $x = 0$, can be decomposed as a sum of a chemical strain, $\varepsilon_i^0(x)$, that emerges from a change in crystal dimensions as Li is added to the crystallite and an elastic strain due to coherency constraints, ε_i

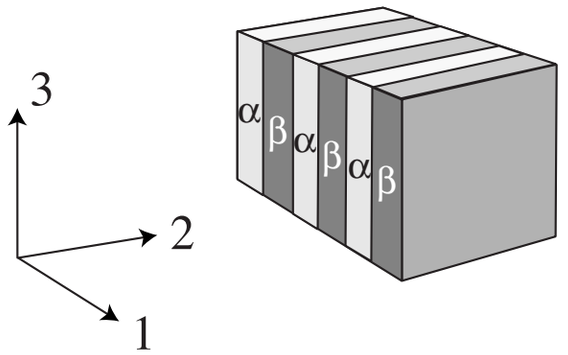

Figure 2. Definition of the coordinate system relative to the periodic two-phase morphology within a rectangular prism crystallite. Axis 1 is perpendicular to the interface between α and β.

$$\tilde{\varepsilon}_i = \varepsilon_i^0(x) + \varepsilon_i \quad [3]$$

The elastic strains result in elastic stresses, which for the orthorhombic crystals of Li_xFePO_4 take the form

$$\sigma_1 = c_{11}\varepsilon_1 + c_{12}\varepsilon_2 + c_{13}\varepsilon_3$$

$$\sigma_2 = c_{21}\varepsilon_1 + c_{22}\varepsilon_2 + c_{23}\varepsilon_3$$

$$\sigma_3 = c_{31}\varepsilon_1 + c_{32}\varepsilon_2 + c_{33}\varepsilon_3$$

$$\sigma_4 = c_{44}\varepsilon_4 \quad \sigma_5 = c_{55}\varepsilon_5 \quad \sigma_6 = c_{66}\varepsilon_6 \quad [4]$$

where the elastic constants, c_{ij}, generally depend on the Li concentration of the host (see, e.g., Ref. 33).

A crystallite having a homogeneous Li concentration, x, has a free energy per interstitial site at its equilibrium volume given by $g(x)$. The Li chemical potential μ for an interstitial host such as $FePO_4$ is related to g according to $\mu = \partial g/\partial x$ and corresponds graphically to the slope of g in a free energy vs a Li concentration plot.

If we consider coherent two-phase coexistence between the α- and β-phases, as illustrated in Fig. 2, neither phase has its equilibrium dimensions as coherency requires that the coexisting phases are stretched or compressed to maintain crystallographic continuity at the interface. Neglecting changes in the shape of the crystallite, the strains are homogeneous, with stretching (contraction) in the 2 and 3 directions of the α (β)-phase. Because the crystal is not constrained on the surfaces perpendicular to the 1 direction, it can relax fully with the stress along 1, thereby equilibrating with the external pressure, which for simplicity we take as zero. This reduces the problem to a plane stress description.

The total free energy of the coherently coexisting phases within the crystallite can be written as

$$G = \phi^\alpha M \cdot g^\alpha(x^\alpha) + \phi^\beta M \cdot g^\beta(x^\beta) + E^{\text{strain}} \quad [5]$$

which is a sum of the free energies of the α- and β-phases at their equilibrium dimensions when unconstrained by coherency plus the total elastic strain energy, E^{strain}, arising from coherency strains. The elastic strain energy corresponds to the changes in energy of the α- and β-phases as they are strained from their equilibrium lattice parameters at concentrations x^α and x^β to a common lattice parameter to ensure coherency at the interface. Neglected in the above expression for the total free energy of the crystallite are surface and interfacial free energy terms. These are important for small crystallites,[40,41] but relative to volume contributions to the free energy are small for large crystallites.

Assuming homogeneous strains, we can calculate an expression for the strain energy analytically. The elastic strain energy in the absence of shear strains for an orthorhombic crystallite under plane stress becomes

$$E^{\text{elastic}} = \frac{1}{2}\int_{V_0} [\sigma_2\varepsilon_2 + \sigma_3\varepsilon_3]dV_0 = \frac{1}{2}\int_{V_0} [\tilde{c}_{22}(\varepsilon_2)^2 + 2\tilde{c}_{23}(\varepsilon_2 \cdot \varepsilon_3) + \tilde{c}_{33}(\varepsilon_3)^2]dV_0 \quad [6]$$

where the integral extends over the reference volume V_0 of the crystallite. Here, the plane stress elastic moduli depend on the full matrix of elastic moduli according to

$$\tilde{c}_{ij} = c_{ij} - \frac{c_{1i}c_{1j}}{c_{11}} \quad [7]$$

with $i,j = 1,2,3$. The elastic constants, in principle, depend on the Li concentration. Assuming uniform strain in each phase, the above integral can be written as

$$E^{\text{elastic}} = V_0[\phi^\alpha e^\alpha(\varepsilon_2^\alpha, \varepsilon_3^\alpha) + \phi^\beta e^\beta(\varepsilon_2^\beta, \varepsilon_3^\beta)] \quad [8]$$

where

$$e(\varepsilon_2, \varepsilon_3) = \tfrac{1}{2}[\tilde{c}_{22}(\varepsilon_2)^2 + 2\tilde{c}_{23}(\varepsilon_2 \cdot \varepsilon_3) + \tilde{c}_{33}(\varepsilon_3)^2] \quad [9]$$

should be interpreted as a strain energy density. The total free energy of the crystallite having two-phase coexistence and normalized per interstitial Li site can then be written as

$$\tilde{g}_{\text{coex}} = \frac{G}{M} = \phi^\alpha \tilde{g}^\alpha + \phi^\beta \tilde{g}^\beta \quad [10]$$

where

$$\tilde{g} = g(x) + \Omega e(\varepsilon_2, \varepsilon_3) \quad [11]$$

can be interpreted as the free energy of a homogeneous crystallite per interstitial site having concentration x when the crystallite is elastically strained in the 2 and 3 directions by ε_2 and ε_3 but free to relax in the 1 direction relative to its equilibrium volume at concentration x. In Eq. 11, Ω is the volume of the crystal per Li site (measured in the reference state at $x = 0$), such that V_0/Ω is equal to the total number of interstitial sites. With Eq. 3, the free energy for the strained crystallite can be considered to depend explicitly on the temperature T, the pressure P (which determines the stress along direction 1, σ_1), the Li concentration x, and the total strains $\tilde{\varepsilon}_2$ and $\tilde{\varepsilon}_3$ in the 2 and 3 directions, i.e., $\tilde{g}(T,P,x,\tilde{\varepsilon}_2,\tilde{\varepsilon}_3)$.

Coherent Two-Phase Equilibrium Criteria

We analyze coherent two-phase equilibrium within a rectangular prism crystallite, with the interface separating α and β perpendicular to the 1 direction, all at constant temperature T, pressure P, and constant number of Li ions N. (Because the stress arising from coherency strains is significantly larger than the hydrostatic pressure from the environment, we neglect the role of ambient pressure and take $P = 0$. This also avoids the need for cumbersome Legendre transforms.) The crystallite has several internal degrees of freedom that are not fixed by the experimental boundary conditions. Although the total number of Li ions is constant, their distribution over the coexisting phases α and β is not. We can use N^α as an independent internal metric for the distribution of Li between the coexisting phases ($N^\beta = N - N^\alpha$). The phase fraction of α (or β) within the crystallite is also not imposed by external boundary conditions but sets in at a particular value of ϕ^α in equilibrium ($\phi^\beta = 1 - \phi^\alpha$). Finally, due to coherency constraints, there are also dimensional degrees of freedom in the 2 and 3 directions that are not imposed externally. The total strains, $\tilde{\varepsilon}_2$ and $\tilde{\varepsilon}_3$, relative to the reference volume at $x = 0$ can serve as variables for these degrees of freedom within the assumption of homogeneous deformations within each phase.

In equilibrium, the internal independent degrees of freedom choose values that minimize the total free energy of the two-phase crystallite. This minimum can be determined by setting the partial derivatives of G (Eq. 5) with respect to the independent variables equal to zero

$$\left(\frac{\partial G}{\partial N^{\alpha}}\right)_{\phi^{\alpha},\tilde{\varepsilon}_2,\tilde{\varepsilon}_3} = 0 \quad [12a]$$

$$\left(\frac{\partial G}{\partial \phi^{\alpha}}\right)_{N^{\alpha},\tilde{\varepsilon}_2,\tilde{\varepsilon}_3} = 0 \quad [12b]$$

$$\left(\frac{\partial G}{\partial \tilde{\varepsilon}_2}\right)_{N^{\alpha},\phi^{\alpha},\tilde{\varepsilon}_3} = 0 \quad [12c]$$

$$\left(\frac{\partial G}{\partial \tilde{\varepsilon}_3}\right)_{N^{\alpha},\phi^{\alpha},\tilde{\varepsilon}_2} = 0 \quad [12d]$$

An explicit solution to the above equations leads to four equilibrium criteria for a coherent two-phase equilibrium between α and β within a crystallite

$$\tilde{\mu}^{\alpha} = \tilde{\mu}^{\beta} \quad [13]$$

$$\tilde{g}^{\alpha} - x_{\alpha}\tilde{\mu}^{\alpha} = \tilde{g}^{\beta} - x_{\beta}\tilde{\mu}^{\beta} \quad [14]$$

$$\phi^{\alpha}\sigma_2^{\alpha} + \phi^{\beta}\sigma_2^{\beta} = 0 \quad [15]$$

$$\phi^{\alpha}\sigma_3^{\alpha} + \phi^{\beta}\sigma_3^{\beta} = 0 \quad [16]$$

In Eq. 13, the lithium chemical potential $\tilde{\mu}^{\xi}$, where ξ refers to either the α or β phase, is derived from the free energies $\tilde{g}^{\xi}$ defined in Eq. 11 of the strained crystallite at constant $\tilde{\varepsilon}_2$ and $\tilde{\varepsilon}_3$ (i.e., constant lateral dimensions in the 2 and 3 directions) according to

$$\tilde{\mu}^{\xi} = \left(\frac{\partial \tilde{g}^{\xi}}{\partial x^{\xi}}\right)_{\tilde{\varepsilon}_2,\tilde{\varepsilon}_3} \quad [17]$$

The Li chemical potential can be written explicitly as

$$\tilde{\mu}^{\xi} = \frac{\partial g^{\xi}}{\partial x^{\xi}} + \frac{\Omega}{2}\left[(\varepsilon_2^{\xi})^2\frac{\partial \tilde{c}_{22}^{\xi}}{\partial x^{\xi}} + 2(\varepsilon_2^{\xi}\cdot\varepsilon_3^{\xi})\frac{\partial \tilde{c}_{23}^{\xi}}{\partial x^{\xi}} + (\varepsilon_3^{\xi})^2\frac{\partial \tilde{c}_{33}^{\xi}}{\partial x^{\xi}}\right] - \Omega\sum_{i=2}^{3}\frac{\partial e^{\xi}}{\partial \varepsilon_i^{\xi}}\frac{\partial \varepsilon_i^{0\xi}}{\partial x^{\xi}} \quad [18]$$

accounting for the possibility that the elastic moduli and lattice parameters depend on the Li concentration. The stresses appearing in Eq. 15 and 16 are related to the strain energy densities according to

$$\sigma_i^{\xi} = \left(\frac{\partial e^{\xi}}{\partial \varepsilon_i^{\xi}}\right)_{x^{\xi},\varepsilon_{j\neq i}^{\xi}} = \left(\frac{\partial \tilde{g}^{\xi}}{\partial \tilde{\varepsilon}_i}\right)_{x^{\xi},\tilde{\varepsilon}_{j\neq i}} \quad [19]$$

where the second equality emerges because the free energy g, appearing in Eq. 11 and corresponding to the free energy of the crystal at its equilibrium volume, does not depend on $\tilde{\varepsilon}_2$ and $\tilde{\varepsilon}_3$. Equations 15 and 16 are the mathematical statements that the average stresses of the crystallite in the 2 and 3 directions are zero. In view of the second equality in Eq. 19, the mechanical equilibrium criteria, Eq. 15 and 16, for two-phase coexistence can be expressed in terms of $\tilde{g}_{\mathrm{coex}}$, defined by Eq. 10, according to

$$\left(\frac{\partial \tilde{g}_{\mathrm{coex}}}{\partial \tilde{\varepsilon}_i}\right)_{x^{\alpha},x^{\beta},\tilde{\varepsilon}_{j\neq i}} = \phi^{\alpha}\left(\frac{\partial \tilde{g}^{\alpha}}{\partial \tilde{\varepsilon}_i}\right)_{x^{\alpha},\tilde{\varepsilon}_{j\neq i}} + \phi^{\beta}\left(\frac{\partial \tilde{g}^{\beta}}{\partial \tilde{\varepsilon}_i}\right)_{x^{\beta},\tilde{\varepsilon}_{j\neq i}} = 0 \quad [20]$$

where implicitly the overall concentration x is also held constant during differentiation. In general, because equilibrium lattice parameters and elastic moduli may depend on concentration, the mechanical equilibrium criteria, Eq. 15 and 16, depend on the chemical equilibrium criteria, Eq. 13 and 14, and vice versa, and all four equations need to be solved simultaneously.

At constant $\tilde{\varepsilon}_2$ and $\tilde{\varepsilon}_3$, the chemical equilibrium criteria, Eq. 13 and 14, are equivalent to the well-known common tangent construction for the two-phase equilibrium applied to $\tilde{g}^{\alpha}$ and $\tilde{g}^{\beta}$. For interstitial intercalation compounds, such as Li_xFePO_4, that maintain the same host crystal structure over the whole concentration range, the free energy of the homogeneous phase is one continuous curve as a function of x. This is illustrated schematically in Fig. 3. The free energy $\tilde{g}^{\alpha}$ then denotes the free energy of Li_xFePO_4 corresponding to the Li-poor free energy well (α-phase), while $\tilde{g}^{\beta}$ denotes the free energy of Li_xFePO_4 for the Li-rich free energy well (β-phase). Equation 13 requires that the slopes to $\tilde{g}^{\alpha}$ and $\tilde{g}^{\beta}$ at x^{α} and x^{β} are parallel, while Eq. 14, which corresponds to an equality of grand canonical potentials, requires that the tangents to $\tilde{g}^{\alpha}$ and $\tilde{g}^{\beta}$ at x^{α} and x^{β} intersect the $\tilde{g}$-axis at $x = 0$ at the same point. The total free energy per interstitial site, $\tilde{g}_{\mathrm{coex}}$, resides on the common tangent at the bulk concentration x, as illustrated in Fig. 3. The mechanical equilibrium criteria, Eq. 15 and 16, expressed in the form of Eq. 20, requires that the normalized free energy of the two-phase crystallite $\tilde{g}_{\mathrm{coex}}$ (Eq. 10) at the bulk concentration x is minimum with respect to variations in the lateral dimensions $\tilde{\varepsilon}_2$ and $\tilde{\varepsilon}_3$ of the crystallite. The corresponding matrix of second derivatives $(\partial^2\tilde{g}_{\mathrm{coex}}/\partial\tilde{\varepsilon}_i\,\partial\,\tilde{\varepsilon}_j)$ is positive definite because the strain energy densities, e^{α} and e^{β}, are convex by construction. The extrema are therefore minima.

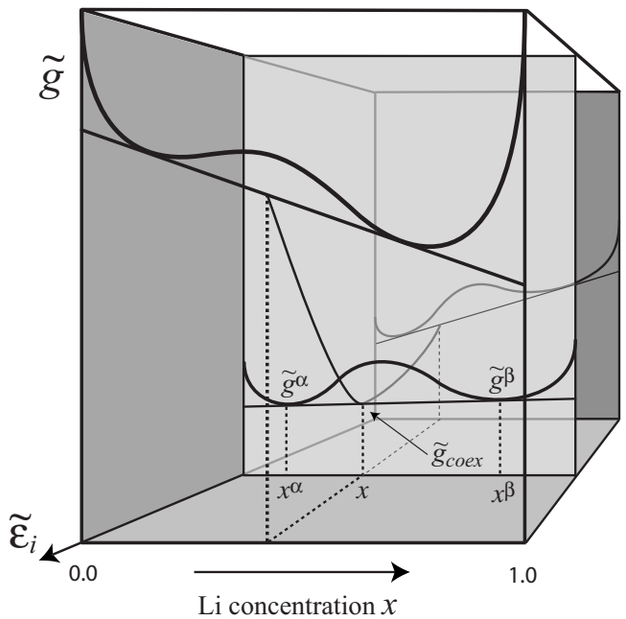

Figure 3. Graphical construction to determine coherent two-phase coexistence, including the effect of strain. Chemical equilibrium is determined by the common tangent construction at fixed strains $\tilde{\varepsilon}_2$ and $\tilde{\varepsilon}_3$. $\tilde{g}_{\mathrm{coex}}$ resides on the common tangent at the overall crystallite concentration x. Mechanical equilibrium is then determined by a minimum of $\tilde{g}_{\mathrm{coex}}$ with respect to strains $\tilde{\varepsilon}_2$ and $\tilde{\varepsilon}_3$. In a coherent two-phase crystallite, the equilibrium strains $\tilde{\varepsilon}_2$ and $\tilde{\varepsilon}_3$ therefore depend on the composition x.

The four equilibrium criteria and their graphical interpretation of Fig. 3 clearly illustrate an important difference with incoherent two-phase equilibrium, as discovered by Cahn and Larche,[25] Williams,[21,22] and Voorhees and Johnson.[30] For incoherent two-phase equilibrium, the concentrations of the coexisting phases x^{α} and x^{β} are independent of the overall concentration x, and the Li chemical potential remains constant as x is varied between x^{α} and x^{β}. For coherent two-phase equilibrium, in contrast, x^{α} and x^{β} are not necessarily constant, and the Li chemical potential varies with the overall concentration x. This arises from the fact that the free energies, $\tilde{g}^{\alpha}$ and $\tilde{g}^{\beta}$, and chemical potentials, $\tilde{\mu}^{\alpha}$ and $\tilde{\mu}^{\beta}$, of Eq. 12 and 13 depend on the lateral dimensions, $\tilde{\varepsilon}_2$ and $\tilde{\varepsilon}_3$, of the α- and β-phases, which vary with x.

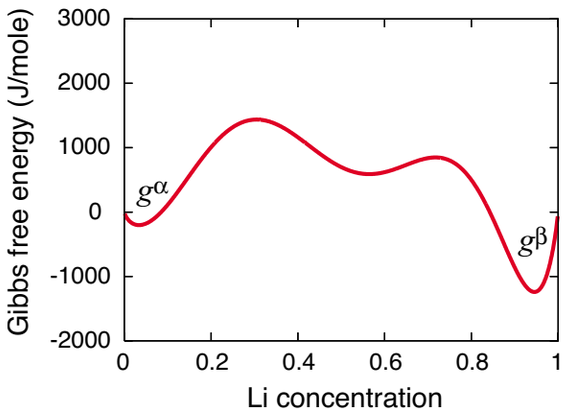

Figure 4. (Color online) Model free energy curve for Li_xFePO_4 parametrized by adjusting the coefficients of the voltage curve derived from the empirical free energy model (Eq. 21) to experimental measurements.[43]

Application to Li_xFePO_4

While Li_xFePO_4 at room temperature appears to have thermodynamic properties similar to that of a regular solution model, exhibiting a miscibility gap between crystallographically identical host structures with different Li compositions, its thermodynamic properties are significantly more complex as manifested by its high temperature behavior.[17,18,37] Delacourt et al.[17] and Dodd et al.,[18] for example, showed that Li_xFePO_4 becomes a solid solution at high temperature, but the phase diagram at intermediate temperatures is qualitatively different from that of a simple miscibility gap. At around 200°C, Li_xFePO_4 solid solutions decompose to Li-poor $Li_\delta FePO_4$ and Li-rich $Li_{1-\varepsilon}FePO_4$ through a eutectoid reaction with a eutectoid composition $x = 0.6$. Hence, the free energy curve, even at room temperature, is likely to differ from that of a simple regular solution model. To have an accurate model for the free energy of Li_xFePO_4, we used an empirical free energy expression commonly used in calculation of phase diagrams (CALPHAD) descriptions of experimental thermodynamic data, relying on a Redlich–Kister polynomial expansion[42] of the excess free energy along with an ideal-solution configurational entropy term (for both Li-vacancy disorder and localized electron disorder). The free energy for Li_xFePO_4 can then be written according to

$$g(x) = g_0(1-x) + g_1 \cdot x + x(1-x)\sum_{n=0}^{m} L_n(1-2x)^n + 2RT[x\ \ln\ x + (1-x)\ln(1-x)] \quad [21]$$

where g_0 and g_1 are the free energies of $FePO_4$ and $LiFePO_4$, and L_n are coefficients of the Riedlich–Kister polynomial expansion. Terms up to order $n = 5$ were included. The factor of 2 in front of the ideal-solution entropy expression arises from the fact that for every Li site that can accommodate Li-vacancy disorder, there is also an Fe site that can accommodate localized electron–hole disorder.[37] The coefficients of the Redlich–Kister expansion were adjusted to produce an open cell voltage curve similar to that measured by Meethong et al.[43] and also to ensure that two-phase coexistence is predicted, even in the presence of coherency strains. No attempt, however, was made to perform an in-depth CALPHAD-like assessment as voltage curves for true bulk phases of Li_xFePO_4 with negligible surface and interface contributions are unlikely available. The resulting free energy at room temperature is illustrated in Fig. 4. We point out the existence of a local minimum in the free energy curve around $x = 0.55$. This feature in the free energy, while an artifact of matching a high order polynomial to thermodynamic data for dilute and concentrated Li_xFePO_4 at room temperature, is not inconsistent with the eutectoid reaction at 200°C whereby the α/β two-phase mixture decomposes into the intermediate solid solution phase, Li_xFePO_4, with $x \sim 0.6$, upon heating.

In treating coherent two-phase coexistence in Li_xFePO_4, we make two assumptions to simplify the analysis: (*i*) the elastic moduli are independent of the Li concentration and (*ii*) the lattice parameters obey Vegard's law (linear dependence of the lattice parameters on Li concentration). Vegard's law for the lattice parameters implies that the chemical strains have the form

$$\varepsilon_i^{0\alpha}(x^\alpha) = \tau_i \cdot x^\alpha \quad \text{and} \quad \varepsilon_i^{0\beta}(x^\beta) = \tau_i \cdot x^\beta \quad [22]$$

In Eq. 22, τ_i has the same value in both the α- and β-phases. As a quantitative estimate of realistic elastic moduli, we used values predicted from first principles, taking the average of each c_{ij} for $FePO_4$ and $LiFePO_4$.[33]

With these assumptions, a solution to the mechanical equilibrium criteria, Eq. 15 and 16, is possible without simultaneously having to consider the chemical equilibrium criteria, yielding

$$\tilde{\varepsilon}_i = \tau_i x \quad [23]$$

for the total strains of the crystallite in the lateral dimensions 2 and 3. As Eq. 23 shows, the lateral dimensions of the crystallite now only depend on the overall Li concentration of the crystallite, x, and not independently of the phase fractions or Li concentrations in the α- and β-phases. Within each phase, the elastic strains in the 2 and 3 directions become, using Eq. 3, 22, and 23

$$\varepsilon_i^\alpha = -\tau_i(x^\alpha - x) \quad \text{and} \quad \varepsilon_i^\beta = -\tau_i(x^\beta - x) \quad [24]$$

This expression shows that the elastic strains in the coexisting phases depend on the difference in the concentration of each phase relative to the overall Li concentration of the crystallite.

With Eq. 22 and 24 and constant $\tilde{c}_{ij}$, we can write the Li chemical potential in coherent two-phase coexistence (Eq. 18), which for the α-phase, for example, becomes

$$\tilde{\mu}^\alpha(x^\alpha) = \mu^\alpha(x^\alpha) + \Omega\Gamma(x^\alpha - x) \quad [25]$$

while the free energy in coherent two-phase coexistence becomes

$$\tilde{g}^\alpha(x^\alpha) = g^\alpha(x^\alpha) + \frac{\Omega\Gamma}{2}(x^\alpha - x)^2 \quad [26]$$

where Γ is a function of the elastic constants and τ_i of Eq. 22

$$\Gamma = \tilde{c}_{22}\tau_2^2 + 2\tilde{c}_{23}\tau_2 \cdot \tau_3 + \tilde{c}_{33}\tau_3^2 \quad [27]$$

Similar expressions hold for $\tilde{\mu}^\beta$ and $\tilde{g}^\beta$. Although the expressions for $\tilde{\mu}^\alpha$ and $\tilde{g}^\alpha$ ($\tilde{\mu}^\beta$ and $\tilde{g}^\beta$) take a simple form, they still depend explicitly not only on x^α (x^β) but also on the overall Li concentration x (because the bulk composition x determines the lateral dimensions $\tilde{\varepsilon}_2$ and $\tilde{\varepsilon}_3$). Hence, as the overall concentration of the crystallite, x, is varied within the two-phase region, the coherent two-phase equilibrium free energies, $\tilde{g}^\alpha$ and $\tilde{g}^\beta$, also change. Cahn[20] presented similar expressions for a cubic crystal in his study of coherent equilibrium close to the critical point of a binary miscibility gap.

With Eq. 22 and 23, the chemical equilibrium criteria for coherent two-phase coexistence, Eq. 13 and 14, reduce to a simple common tangent construction in a free energy vs Li composition plot. This is illustrated in Fig. 5a and b for morphology I (Fig. 1) in which the interface between α and β is parallel to the *bc* plane. For morphology I, we take the *a* lattice vector of the orthorhombic crystal to be aligned with axis 1, the *b* lattice vector along axis 2, and the *c* lattice vector parallel to axis 3. The misfit strains are taken to be $\tau_2 = 0.036$ and $\tau_3 = -0.0186$ based on the experimentally measured difference in lattice parameters between $FePO_4$ and $LiFePO_4$ in the *b*- and *c*-directions.[13] Figure 5a and b illustrates how the free energy in coherent two-phase equilibrium, $\tilde{g}$ of Eq. 26, depends on the overall crystallite concentration x, with Fig. 5a showing $\tilde{g}$ at $x = 0.3$ and Fig. 5b showing $\tilde{g}$ at $x = 0.7$. The free energies corresponding to the free energy wells in the Li-poor and Li-rich regions are referred to as $\tilde{g}^\alpha$ and $\tilde{g}^\beta$, respectively, as illustrated in Fig. 5, even though they reside on a single free energy curve $\tilde{g}$. The total

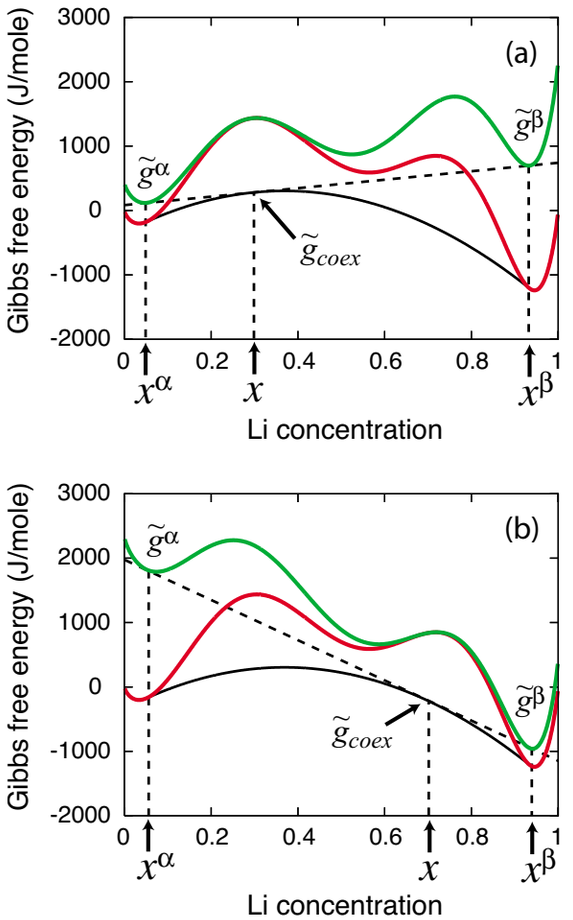

Figure 5. (Color online) Illustration of the common tangent construction for coherent two-phase equilibrium in the special case that the elastic moduli are independent of concentration and the lattice parameters vary linearly with concentration. (Color: The middle red free energy curve is for the homogeneous phase, while the top green free energy curve corresponds to $\tilde{g}$).

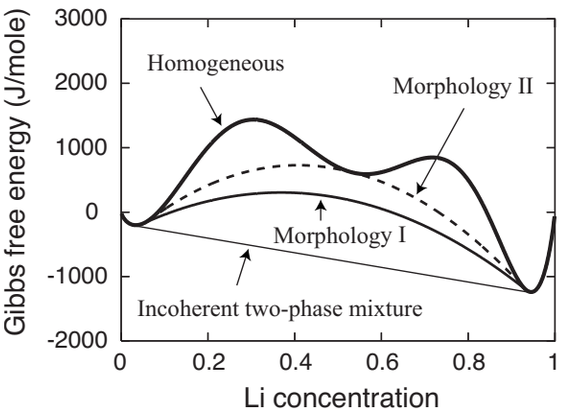

Figure 6. Free energy for two-phase coexistence for the various morphologies of Fig. 1.

free energy of the crystallite per formula unit for the two-phase equilibrium state, $\tilde{g}_{\text{coex}}$, given by Eq. 10, lies on the common tangent to $\tilde{g}^{\alpha}$ and $\tilde{g}^{\beta}$ at the overall crystallite concentration x. The black curve in Fig. 5a and b corresponds to the envelope of the coexistence free energy $\tilde{g}_{\text{coex}}$ as a function of x.

Effect of coherency strain on solubility limits.— We can assess the importance of coherency strain energy in altering the concentrations within the coexisting phases x^{α} and x^{β}. In the absence of coherency strains (i.e., equivalent to incoherent two-phase equilibrium), these concentrations for Li_xFePO_4 for our free energy model illustrated in Fig. 4 are $x^{\alpha} = 0.03$ and $x^{\beta} = 0.94$. With the inclusion of coherency strain energy, the concentrations within the coexisting phases change to $x^{\alpha} = 0.05$ and $x^{\beta} = 0.93$. Hence, the effect of coherency strain energy on the concentrations of coexisting phases for our free energy model of Li_xFePO_4 is quite small, changing them by 1–2%. For the assumptions made here (constant elastic moduli and linear concentration dependence of the lattice parameters), the concentrations, x^{α} and x^{β}, happen to be independent of x, as was shown by Lee and Tao.[44] However, relaxing these assumptions results in compositions x^{α} and x^{β} that vary with the bulk concentration x.

Effect of coherency strain on two-phase morphologies.— Figure 6 illustrates free energies per interstitial site for the different morphologies of two-phase coexistence of Fig. 1. For incoherent two-phase coexistence (in the absence of coherency strains), the normalized free energy (per Li interstitial site) resides on the common tangent to the free energy of the homogeneous phase. This free energy is the weighted sum of the free energies of α and β in their unstrained states. The free energy of coherent two-phase coexistence is always higher than that of incoherent coexistence due to the presence of a coherency strain energy penalty. The solid line in Fig. 6 corresponds to the free energy, $\tilde{g}^{\text{I}}_{\text{coex}}$, of coherent two-phase coexistence with morphology I (Fig. 1) in which the interface is oriented parallel to the *bc* plane. The dashed line denoted $\tilde{g}^{\text{II}}_{\text{coex}}$ corresponds to the coherent two-phase coexistence free energy for morphology II with the interface parallel to the *ac* plane. For morphology II of Fig. 1, the *b* lattice vector is parallel to axis 1, the *c* lattice vector is parallel to axis 2, and the *a* lattice vector is parallel to axis 3. The misfit strains for this morphology are then $\tau_2 = -0.0186$ and $\tau_3 = 0.052$ based on changes in lattice parameters between $FePO_4$ and $LiFePO_4$.[13]

Figure 6 clearly shows that morphology I has a lower free energy than morphology II, consistent with experimental observations of two-phase coexistence with the interface perpendicular to the *a*-direction.[13] In morphology I, the *a* lattice parameter, which undergoes the largest change when transforming from $FePO_4$ to $LiFePO_4$, is able to fully relax, while in morphology II, the lattice parameters *a* of coexisting α and β must be constrained to a common value.

Coherency strain and low temperature stabilization of high temperature solid solutions.— In Fig. 6, $\tilde{g}^{\text{II}}_{\text{coex}}$ merges with the local minimum of the homogeneous free energy around $x = 0.55$. This local minimum corresponds to a metastable phase around $x = 0.55$, which we shall call the γ-phase. The local minimum is an artifact of using a high order polynomial when fitting an empirical free energy expression (Eq. 21) to the voltage profile for single-phase α and β. Nevertheless, due to the experimentally observed eutectoid reaction around 200°C,[18] where Li_xFePO_4 at $x \sim 0.6$ emerges from the decomposition of a two-phase mixture of α-$FePO_4$ and β-$LiFePO_4$, it is likely that such a local minimum exists in the actual free energy of Li_xFePO_4 at room temperature. The implication of Fig. 6 is that if coherent two-phase coexistence is only permitted to occur according to morphology II, the γ-phase around $x = 0.55$ can be thermodynamically stabilized at room temperature. This emerges because any coherent two-phase separation into α and β along the *b*-direction at $x \sim 0.55$ has a higher free energy than the metastable γ-phase. For coherent two-phase coexistence with morphology II, Fig. 6 predicts that a two-phase mixture between α and γ occurs below $x \sim 0.55$, while above $x \sim 0.55$ a coherent two-phase mixture between γ and β is stable.

Although morphology II has a higher strain energy penalty than morphology I, the fact that Li diffusion can only occur along the *b*-axis in Li_xFePO_4 can lead to scenarios where two-phase decom-

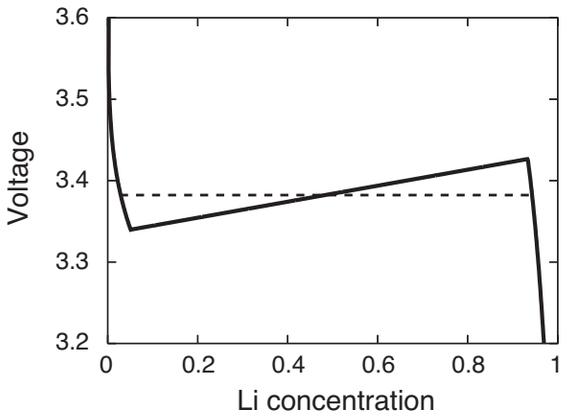

Figure 7. Voltage curve for a single crystallite. The dashed line corresponds to the voltage plateau of incoherent two-phase equilibrium, while the increasing sloped solid line is the voltage during coherent two-phase equilibrium having morphology I of Fig. 1.

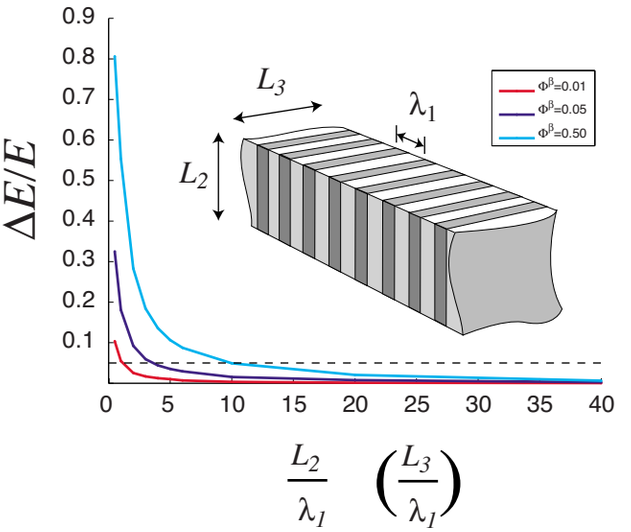

Figure 8. (Color online) Relative error of the analytical approximation for a periodic two-phase coexistence as a function of the crystallite dimensions relative to the periodicity of the two-phase morphology. The dashed line indicates a relative error of 5%.

position is kinetically only feasible according to morphology II. The formation of morphology I requires selective Li extraction from the surface of the crystallite, such as that proposed by the domino-cascade model,[19] either electrochemically or through chemical oxidation, as Li redistribution along the *a*-direction is not possible within the interior of a Li_xFePO_4 crystallite. If, however, a crystallite with a homogeneous Li distribution at high temperature was subsequently quenched to room temperature in air, it would only be able to redistribute Li along the one-dimensional diffusion channels parallel to the *b*-axis, thereby leading to morphology II (excluding surface diffusion as a possible redistribution mechanism). Chen et al.[34] recently performed these experiments and found with TEM analysis that high temperature intermediate compositions such as $Li_{0.6}FePO_4$ can be quenched to room temperature and remain stable over time. Furthermore, they observed two-phase coexistence similar to that of morphology II of Fig. 1, stating that their "results indicate that upon cooling, the solid solution disproportionates into the fully lithiated phase and a partially lithiated intermediate phase via lithium-ion movement along the *b*-direction, with phase boundaries lying in the *ac* plane."[34]

Coherency strains and voltage.— Although the effect of coherency strain energy on solubility limits is small for olivine Li_xFePO_4 when using our empirical free energy model, its effect is more significant on the voltage curve. In the absence of coherency strains, the voltage within a two-phase region is constant, as the thermodynamic properties of coexisting phases do not change with a variation in the overall concentration; only their phase fraction changes. With coherency strains, the state of strain of the coexisting phases continuously evolves with x due to a variation in the relative phase fractions of the two phases. The intrinsic voltage is related to the Li chemical potential in the crystallite ($\mu_{Li}^{cathode}$) according to

$$V(x) = -(\mu_{Li}^{cathode} - \mu_{Li}^{anode})/eF$$

where μ_{Li}^{anode} is a constant reference chemical potential (e.g., of metallic Li) and F is Faraday's constant (needed if the chemical potentials are expressed in joules).

Figure 7 illustrates the voltage curve for Li_xFePO_4 derived from the above described free energy model. This voltage curve is strictly for a single crystallite when the bulk concentration of the crystallite is controlled externally (e.g., by controlling the current). Upon charging the particle, the voltage must be reduced below the incoherent two-phase equilibrium voltage (dashed line in Fig. 7) to overcome the strain energy incurred by coherent two-phase equilibrium. Hence, the system follows the metastable voltage curve of the Li-poor phase until the thermodynamic driving force for two-phase coexistence is larger than the coherency strain energy incurred by that coexistence. As the overall concentration of the crystallite is increased once inside the coherent two-phase region, the phase fraction of the Li-rich phase increases at the expense of the Li-poor phase. Due to coherency, a change in the relative fractions of the Li-rich and Li-poor phases changes the lateral dimensions of the crystallite, thereby making the voltage dependent on the bulk concentration of the crystallite within the two-phase region. When assuming constant elastic moduli and Vegard's law, the voltage for a single crystallite increases linearly inside the two-phase region. Similar behavior was predicted for the hydrogen partial pressure during hydrogen sorption in Pd.[31,32]

Discussion

An important approximation in our analytical treatment of elasticity was to assume that the crystallite does not change shape but only expands or contracts along the three axes parallel to the crystallographic lattice vectors. In reality, the shape of the crystallite changes during the two-phase coexistence with some degree of surface rumpling. Chen et al.[13] observed slight rotations of coexisting phases relative to each other. The analytical coherency strain energy therefore serves as an upper bound to the coherency strain energy in real crystallites as it is derived assuming restricted deformational degrees of freedom. The analytical treatment becomes more accurate if the two-phase morphology is periodic, as illustrated in Fig. 1 and 2, and systematically improves as the periodicity between α and β domains along the 1 direction reduces relative to the dimensions of the crystallite in the 2 and 3 directions. This is illustrated in Fig. 8 where the coherency strain energy for three different phase fractions of α, obtained from a finite element calculation that allows the shape of the crystallite to change, is compared to the analytical coherency strain energy used in our thermodynamic analysis. In the analytical and finite element treatment of Fig. 8, different elastic moduli were used for the α- and β-phases, as predicted from first principles.[33]

X-ray diffraction measurements by Chen et al.[34] show that coexisting $LiFePO_4$ and $FePO_4$ have different lattice parameters, implying that coherent equilibrium is relaxed to some extent. In actual crystallites, the strain is not uniform throughout each individual phase. A more rigorous treatment of coherent two-phase equilibrium would then require the introduction of field variables for the local concentration and strains followed by an integration over the local strain energy and chemical free energy to obtain the total free energy

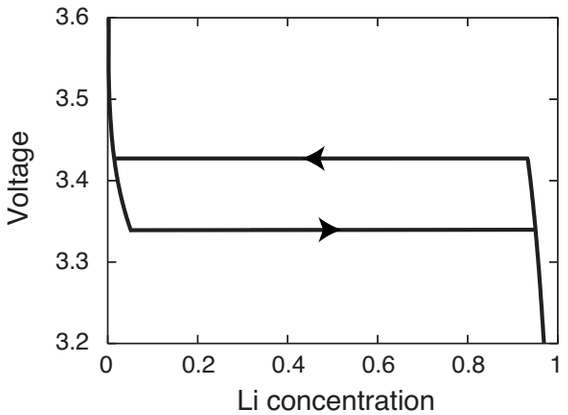

Figure 9. Voltage profile accounting for the role of coherency strains when the voltage (as opposed to the Li concentration) is externally controlled.

of the crystallite. Equilibrium criteria then emerge after taking variational derivatives of the total free energy with respect to the concentration and strain fields as well as the interface shape separating α from β.[26,30]

The most important result of the analytical treatment from an experimental point of view is the effect of coherency strain energy on the compositions of the coexisting phases and on the overpotential required to initiate the transformation from α to β (or vice versa). These are determined by the coherency strain energy associated with a very small phase fraction of the new phase. As is clear in Fig. 8, the analytical treatment becomes a better approximation as the phase fraction of the minor phase diminishes.

The voltage profile of Fig. 7 for coherent two-phase equilibrium is strictly valid for individual crystallites when the concentration of the crystallite is controlled externally (e.g., by controlling the current). While voltages are usually measured at a constant current, electrochemical measurements can also be performed controlling the voltage, which, in thermodynamic equilibrium, imposes a constant Li chemical potential on the system as opposed to a constant number of Li ions. Under this constraint, the voltage vs composition profile has a different appearance, exhibiting hysteresis, as illustrated in Fig. 9. When discharging an electrode that transforms coherently, for example, the voltage must be reduced sufficiently below the incoherent two-phase equilibrium voltage plateau to overcome the energy penalty of coherency strains. Once that underpotential has been reached, the crystallite at the constant external voltage transforms irreversibly to the Li-rich phase at the same voltage. Upon charging, a similar overpotential must be exceeded in the opposite direction to overcome coherency strain energy of two-phase coexistence, after which the system irreversibly transforms to the Li-poor phase if the voltage is externally controlled. Hence, coherency strains, when controlling the voltage, lead to losses as the builtup elastic strain energy that must be overcome is released to the environment in an irreversible manner (e.g., sound waves, crack, and dislocation formation).

Even if the concentration of the electrode is externally controlled, it is unlikely that the qualitative voltage profile of Fig. 7 is observed in actual electrochemical cells as electrodes consist of many crystallites, allowing Li ions to redistribute between the different crystallites. If, for example, a situation were reached where all particles had the same concentration inside the coherent two-phase region, then the overall free energy of the composite electrode would be minimized by having some crystallites give up Li and become a single-phase Li-poor crystallite and other crystallites accumulate more Li and become single phase but Li rich. This is equivalent to incoherent two-phase equilibrium without the coherency strain energy penalty. In equilibrium, the voltage would then coincide with that for incoherent two-phase equilibrium (neglecting

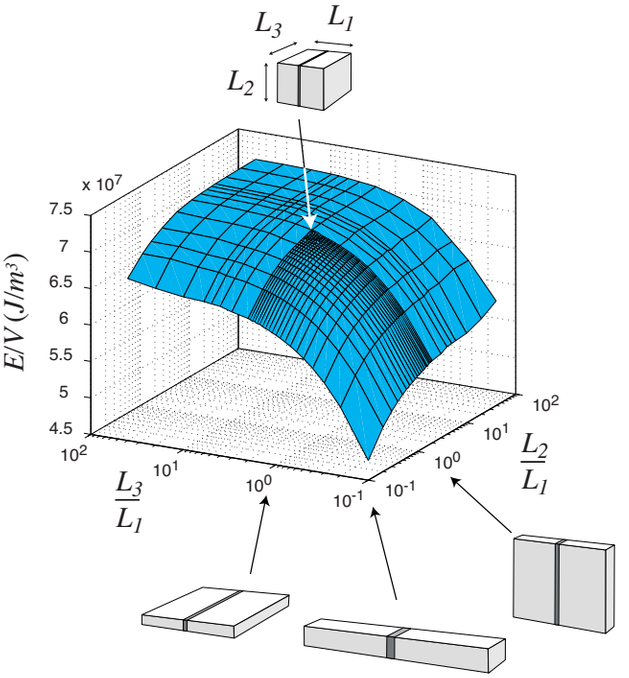

Figure 10. (Color online) Coherency strain energy density as a function of crystallite dimensions when the α-phase forms at the center of a pre-existing β crystallite (a 1% phase fraction of α is assumed).

surface energy terms). Nevertheless, upon addition of Li, a subset of crystallites must transform from the Li-poor phase to the Li-rich phase, and the transformation involves the temporary existence of coherent two-phase equilibrium. Before this is possible, an underpotential (overpotential) is required to overcome the strain energy arising from coherent two-phase equilibrium. However, the collection of electrode crystallites again relaxes to a collection of coexisting single-phase crystallites, as has recently been observed experimentally.[45]

We emphasize that the quantitative as well as qualitative predictions of the current treatment are sensitive to the behavior of the free energy of the homogeneous phase inside the incoherent two-phase region. This portion of the free energy of Li_xFePO_4, which in our free energy model is simply a polynomial extrapolation, is currently not known and very difficult to access experimentally. The effect of coherency strain on the compositions of the coexisting phases, x^α and x^β, will be more significant than predicted here if the difference between the homogeneous free energy inside the two-phase region and the common tangent, Δg, is smaller than in the free energy model for Li_xFePO_4 used in the present study. In fact, two-phase coexistence could be completely suppressed within individual crystallites at room temperature if the maximum value of Δg inside the two-phase region is less than the coherency strain energy penalty of two-phase coexistence.

The coherency strain energy scales with the size of the crystallite and depends on the crystallite shape. For macroscopic crystallites, this coherency strain energy is too large to be overcome by thermal fluctuations, and two-phase coexistence can only be achieved by a large overpotential in the voltage, as described above. One way to reduce the overpotential needed to initiate two-phase coexistence in macroscopic crystallites is by adjusting the crystallite shape in a way that minimizes the coherency strain energy introduced upon nucleating the new phase. Figure 10 illustrates the coherency strain energy density (strain energy divided by the volume of the crystallite) for a rectangular prism when a thin α-phase (phase fraction of 1%) exists at the center of a β crystallite. The interface is taken to be in the *bc* plane, perpendicular to *a*. The strain energy density was

obtained from finite element computations, allowing the shape of the crystallite to relax and using elastic moduli for α and β predicted from first principles.[33] The strain energy density is plotted as a function of the crystallite lengths in the 2 and 3 directions relative to the crystallite length in the 1 direction. The minimal strain energy associated with nucleating a thin slice of the new phase occurs for long, needlelike crystallites where lengths L_2 and L_3 are significantly shorter than length L_1. In this geometry, the strain energy resulting from the lattice mismatch along the *b* and *c* lattice vectors is minimized because the interface area across which the mismatch occurs is minimized.

A minimization of the coherency strain energy through particle shape optimization not only leads to a reduction in the overpotential required to initiate the phase transformation from α to β (or vice versa), but also reduces the likelihood of mechanical damage and fatigue. Large localized stresses during two-phase coexistence can result in the formation of irreversible defects such as dislocations and cracks.[38] These extended crystalline defects hamper the subsequent passage of interfaces during α- to β-phase transformations and result in overall particle degradation. As the crystallites approach the nanoscale, the total coherency strain energy becomes small as well. At very small scales, the coherency strain energy may become comparable to thermal energy and could then be overcome by thermal fluctuations. Hence, at the nanoscale, less of an overpotential is needed to initiate the α- to β-phase transformation. This appears to be confirmed by size dependent electrochemistry measurements, where crystallites with linear dimensions ~110 nm display a (dis)charge curve with an overpotential, whereas smaller particles around 40 and 27 nm do not exhibit this overpotential.[15,16]

Conclusion

We derived mechanochemical equilibrium criteria for two-phase coexistence within Li_xFePO_4 crystallites and analyzed the role of coherency strains in affecting solubility limits, phase stability, and overpotentials required to initiate first-order phase transformations during (dis)charging. We have also shown how coherency strains can stabilize high temperature solid solution phases at low temperature when phase separation is restricted to occur along the Li diffusion direction of the olivine Li_xFePO_4 crystal structure. A finite element analysis shows that the crystallite shape that minimizes the coherency strain for the nucleation of two-phase coexistence has a needle shape with the long axis parallel to the *a*-direction of the olivine crystal structure.

Acknowledgments

Van der Ven acknowledges support from General Motors. K.G. acknowledges support from the Department of Energy Presidential Early Career Award for Scientists and Engineers (PECASE). Financial support from The Netherlands Organization for Scientific Research (NWO) is acknowledged for the CW-VIDI grant of M.W.

University of Michigan assisted in meeting the publication costs of this article.

References

1. P. Oliva, J. Leonardi, J. F. Laurent, C. Delmas, J. J. Braconnier, M. Figlarz, F. Fievet, and A. Deguibert, *J. Power Sources*, **8**, 229 (1982).
2. M. M. Thackeray, *Prog. Solid State Chem.*, **25**, 1 (1997).
3. J. M. Tarascon and M. Armand, *Nature (London)*, **414**, 359 (2001).
4. M. S. Whittingham, *Chem. Rev. (Washington, D.C.)*, **104**, 4271 (2004).
5. A. Van der Ven, G. Ceder, M. Asta, and P. D. Tepesch, *Phys. Rev. B*, **64**, 184307 (2001).
6. A. Van der Ven, J. C. Thomas, Q. Xu, B. Swoboda, and D. Morgan, *Phys. Rev. B*, **78**, 104306 (2008).
7. C. Delmas, C. Fouassier, and P. Hagenmuller, *Physica B & C*, **99**, 81 (1980).
8. G. G. Amatucci, J. M. Tarascon, and L. C. Klein, *J. Electrochem. Soc.*, **143**)3), 1114 (1996).
9. A. K. Padhi, K. S. Nanjundaswami, and J. B. Goodenough, *J. Electrochem. Soc.*, **144**, 1188 (1997).
10. A. Van der Ven, M. K. Aydinol, and G. Ceder, *J. Electrochem. Soc.*, **145**, 2149 (1998).
11. Z. H. Chen, Z. H. Lu, and J. R. Dahn, *J. Electrochem. Soc.*, **149**, A1604 (2002).
12. A. Van der Ven, D. Morgan, Y. S. Meng, and G. Ceder, *J. Electrochem. Soc.*, **153**, A210 (2006).
13. G. Chen, X. Y. Song, and T. J. Richardson, *Electrochem. Solid-State Lett.*, **9**, A295 (2006).
14. D. Morgan, A. Van der Ven, and G. Ceder, *Electrochem. Solid-State Lett.*, **7**, A30 (2004).
15. N. Meethong, H. Y. S. Huang, S. A. Speakman, W. C. Carter, and Y. M. Chiang, *Adv. Funct. Mater.*, **17**, 1115 (2007).
16. N. Meethong, H. Y. S. Huang, W. C. Carter, and Y. M. Chiang, *Electrochem. Solid-State Lett.*, **10**, A134 (2007).
17. C. Delacourt, P. Poizot, J. M. Tarascon, and C. Masquelier, *Nature Mater.*, **4**, 254 (2005).
18. J. L. Dodd, R. Yazami, and B. Fultz, *Electrochem. Solid-State Lett.*, **9**, A151 (2006).
19. C. Delmas, M. Maccario, L. Croguennec, F. Le Cras, and F. Weill, *Nature Mater.*, **7**, 665 (2008).
20. J. W. Cahn, *Acta Metall.*, **10**, 907 (1962).
21. R. O. Williams, *Metall. Trans. A*, **11**, 247 (1980).
22. R. O. Williams, *CALPHAD: Comput. Coupling Phase Diagrams Thermochem.*, **8**, 1 (1984).
23. F. Larche and J. W. Cahn, *Acta Metall.*, **21**, 1051 (1973).
24. F. Larche and J. W. Cahn, *Acta Metall.*, **26**, 1579 (1978).
25. J. W. Cahn and F. Larche, *Acta Metall.*, **32**, 1915 (1984).
26. F. C. Larche and J. W. Cahn, *Acta Metall.*, **33**, 331 (1985).
27. W. C. Johnson and P. W. Voorhees, *Metall. Trans. A*, **18**, 1213 (1987).
28. W. C. Johnson and W. H. Muller, *Acta Metall. Mater.*, **39**, 89 (1991).
29. J. Y. Huh and W. C. Johnson, *Acta Metall. Mater.*, **43**, 1631 (1995).
30. P. W. Voorhees and W. C. Johnson, *Solid State Phys.*, **59**, 1 (2004).
31. R. B. Schwarz and A. G. Khachaturyan, *Phys. Rev. Lett.*, **74**, 2523 (1995).
32. R. B. Schwarz and A. G. Khachaturyan, *Acta Mater.*, **54**, 313 (2006).
33. T. Maxisch and G. Ceder, *Phys. Rev. B*, **73**, 174112 (2006).
34. G. Y. Chen, X. Y. Song, and T. J. Richardson, *J. Electrochem. Soc.*, **154**, A627 (2007).
35. T. Maxisch, F. Zhou, and G. Ceder, *Phys. Rev. B*, **73**, 104301 (2006).
36. B. Ellis, L. K. Perry, D. H. Ryan, and L. F. Nazar, *J. Am. Chem. Soc.*, **128**, 11416 (2006).
37. F. Zhou, T. Maxisch, and G. Ceder, *Phys. Rev. Lett.*, **97**, 155704 (2006).
38. H. Gabrisch, J. Wilcox, and M. M. Doeff, *Electrochem. Solid-State Lett.*, **11**, A25 (2008).
39. J. F. Nye, *Physical Properties of Crystals*, Clarendon, Oxford (1985).
40. A. Van der Ven and M. Wagemaker, *Electrochem. Commun.*, **11**, 881 (2009).
41. M. Wagemaker, F. Mulder, and A. Van der Ven, *Adv. Mater.*, **21**, 2703 (2009).
42. M. Hillert, *Phase Equilibria, Phase Diagrams and Phase Transformations: Their Thermodynamic Basis*, Cambridge University Press, Cambridge, UK (1998).
43. N. Meethong, Y.-H. Kao, M. Tang, H.-Y. Huang, W. C. Carter, and Y.-M. Chiang, *Chem. Mater.*, **20**, 6189 (2008).
44. J. K. Lee and W. M. Tao, *Acta Metall. Mater.*, **42**, 569 (1994).
45. K. T. Lee, H. Wang, and L. F. Nazar, *J. Am. Chem. Soc.*, **131**, 6044 (2009).